BioMetals **13:** 325–331, 2000.

Superparamagnetic Magnetite in the Upper Beak Tissue of Homing Pigeons

Marianne Hanzlik[1], Christoph Heunemann[1], Elke Holtkamp-Rötzler[2], Michael Winklhofer[1], Nikolai Petersen[1] & Gerta Fleissner[2]

[1]*Institut für Allgemeine und Angewandte Geophysik, Ludwig-Maximilians-Universität, D-80333 Munich, Germany*
[2]*Zoologisches Institut, Johann-Wolfgang-Goethe-Universität, D-60054 Frankfurt a. M., Germany*
[*]*Author for correspondence (Tel.: ++49 89 2394 4233; Fax: ++49 89 2394 4205; E-mail: petersen@geophysik.uni-muenchen.de)*

Received 14 August 2000; accepted 30 October 2000

Key words: homing pigeon, magnetoreception, SAED analysis, SQUID magnetometer, ZFC-FC curves

Abstract

Homing pigeons have been subject of various studies trying to detect magnetic material which might be involved in magnetic field perception. Here we focus on the upper-beak skin of homing pigeons, a region that has previously been shown to contain nerves sensitive to changes of the ambient magnetic field. We localized Fe^{3+} concentrations in the subcutis and identified the material by transmission electronmicroscopy (TEM) as aggregates of magnetite nanocrystals (with grain sizes between 1 and 5 nm). The particles form clusters of 1–3 μm diameter, which are arranged in distinct coherent elongated structures, associated with nervous tissue and located between fat cells. Complementary low-temperature magnetic measurements confirm the microscopic observations of fine-grained superparamagnetic particles in the tissue. Neither electron-microscopic nor magnetic measurements revealed any single-domain magnetite in the upper-beak skin tissue.

Introduction

Ferromagnetic material is commonly found in many organisms, although it is normally present only in minute amounts. The most prominent example for ferromagnetic material in organisms are magnetotactic bacteria (Blakemore 1975), where intracellular magnetite particles arranged in chains serve as a tool for orientation in the Earth's magnetic field. In other organisms, the role of ferromagnetic inclusions is less clear. Apart from possibly being a by-product of metabolism, they may play a role in the iron household of the organism, or have a particular function as in the case of magnetite dentical capping in chitons (Lowenstamm 1962), or represent the basis of a magnetoreceptor (Ising 1945).

In order to explain the possible function of ferromagnetic material in a particular organism, its composition, grain size, and – most difficult – its exact location and a possible structural arrangement within the host tissue has to be clarified.

Our studies concentrate on homing pigeons, *Columba livia*, which show a homing behavior that can be influenced by magnetic field cues (Holtkamp-Rötzler 1998; for a review see Wiltschko & Wiltschko 1995).

Walcott *et al.* (1979) were the first who detected permanently magnetic material in the pigeon head. They found it in a small, unilateral, innervated piece of tissue between the dura and the skull and identified the concentrated material by Curie temperature measurement as magnetite. When examining the tissue in light and electron microscope, they found it richly supplied with clusters of electron-opaque structures, approximately 0.08 to 0.15 μm long. In similar experiments Presti & Pettigrew (1980) found two regions with inducible magnetic remanence: In the head and the neck musculature of pigeons and there especially

in the complexus muscle and associated fascia. But in contrast to the findings of Walcott *et al.* (1979), Presti & Pettigrew found the remanence to be distributed uniformly throughout the entire head. They could find no visible magnetic structures in the skull but were able to extract highly magnetic, black particles from tissue between the surface of the complexus muscle and the superficial fascia, which they assumed to consist of magnetite.

Neither of these investigations came so far as to resolve size and nature of individual magnetic particles, nor their exact location and structural arrangement within the tissue.

Starting point of our search for ferromagnetic material in homing pigeons were the electrophysiological studies of Semm *et al.* (1984) on pigeons and of Beason & Semm (1987) on bobolinks. These studies suggested that the premaxillary ramus of the median ophtalmic branch of the trigeminal nerve (Figure 1a), which innervates the mechanoreceptors in the skin of the upper beak (Bubien-Waluszewska 1981), may be involved in magnetoreception, similar to the corresponding ros V (superficial ophtalmic ramus) in trouts (Walker *et al.* 1997). Assuming that the hypothetical magnetoreceptor is based on an interaction of the Earth's magnetic field with ferromagnetic particles, we considered the upper-beak tissue a promising candidate in our search for ferromagnetic material.

Materials and methods

Lightmicroscopy

The upper-beak skins of 7 homing pigeons were embedded in paraplast and plastic (Epon) after having been fixed with glutaraldehyde. These samples were cut into serial histological sections (10 μm thickness). In order to localize the postulated magnetic material, which was tentatively assumed to consist of magnetite ($Fe_2^{3+}Fe^{2+}O_4$) or maghemite (γ-$Fe_2^{3+}O_3$), we looked for concentrations of Fe^{3+} using the Prussian Blue (PB) reaction (Tanka & Berschauer 1969). In the presence of Fe^{3+} and HCl, potassium hexacyanoferrate turns into the dark-blue ferric ferrocyanide (we used Kernechtrot for counterdstaining). We applied the PB reagent for 10 min, which turned out to be sufficiently long to yield a clearly visible reaction. Only every second section was stained. If two consecutive PB-stained sections displayed blue spots at corresponding sites, the unstained section in between - which is likely to contain the same structure, but with the original Fe^{3+}-compound was re-embedded and cut into 100 to 200 nm ultra-thin sections for electron microscopy.

Electronmicroscopy

For further analysis of the iron rich granules, we used transmission electron microscopy (TEM, Zeiss EM 10 A and Phillips CM 10). As the ultra-thin sections were not treated with a precontrasting agent, contrasts are mainly due to opaque material. All micrographs and selected area electron diffraction (SAED) analysis were conducted at 100 keV.

Magnetic measurements

The acquisition and demagnetization of an isothermal magnetic remanence (IRM) of the entire upper-beak skin (fresh unfixed tissue) at room temperature were measured with a LETI SQUID magnetometer (magnetic-moment sensitivity: 10^{-7} G cm^{-3}, in SI units 10^{-10} A m^{-2}). The beak skin was cut into three pieces, i.e., a proximal, medial, and distal one.

Low temperature magnetic measurements were conducted using a Quantum-Design MPMS-XL SQUID magnetometer. Here, the sample (section of the upper-beak skin, thickness approx. 1 mm) was embedded in a diamagnetic resin. 'Zero-Field cooled' curves (ZFC) were measured by cooling the sample in zero field, applying a field H at 5 K and then measuring the magnetic moment in the field H while raising the temperature stepwise up to 300 K. Subsequently, the sample was cooled in the same field H ('field cooled', FC-curve) and then measured by the same experimental procedure as described before. ZFC-FC curves were measured for applied fields H of 50, 100, 150, and 200 Oe (4, 8, 12, and 16 kA m^{-1}, respectively). The diamagnetic signal was subtracted and the data normalized. Because of the poor signal-to-noise ratio, the data were smoothed using a running average (window width 5 data points).

To measure the decay of magnetic remanence, the sample was first cooled in zero field. At 5 K the sample was saturated ($H_{appl} = 25$ kOe respectively 2×10^6 A m^{-1}), the field reduced to zero, and then the saturation remanent magnetic moment measured as a function of temperature (Figure 5, inset).

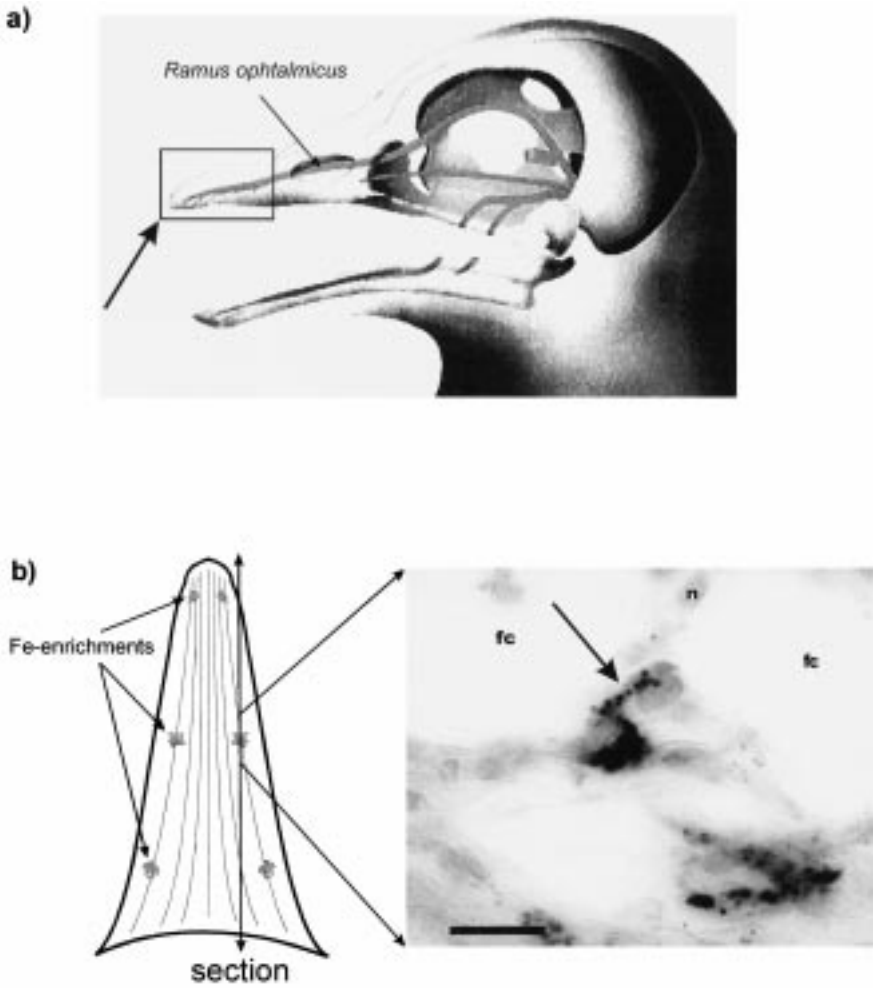

Figure 1. (a) Schematic drawing of the pigeon skull with projections of the cranial nerve. Ramus ophthalmicus is the sensory branch of N. trigeminus that extends to the tip of the upper beak. (b) Left side: Positions of the identified Fe^{3+} accumulations in the upper-beak skin, top view of the inset of Figure 1a. Right side: Light microscopic identification of Fe^{3+} accumulations. Long (sagittal) section stained with Prussian Blue and Kernechtrot. The Fe^{3+} enrichments (indicated by the arrow) form little granules of similar size (1–3 μm), which are aligned in chains along the cells. (Stack of six different focal planes projected into the same plane, by means of the digital microscopic video camera SPOT, enhanced by the Metaview software system.) *fc* fat cell, *n* neurofilament, *scale bar* 10 μm.

Results

Lightmicroscopy

Treating the histological sections with PB, we find up to six isolated sites of Fe^{3+} enrichments in the upper-beak skin, which are symmetrically arranged (Figure 1b, left). The Fe^{3+} enrichment are not randomly distributed in the skin, but always occur in the Stratum laxum of the subcutis within strands of connective tissue, between fat cells (Figure 1b, right) and in association with neurofilaments. The Fe^{3+} enrichments are arranged in sets of cellular elements, which sometimes extend over up to 200 μm. At higher magnification, the PB stained regions are resolved as accumulations of discrete, intensely blue granules of 1 to 3 μm diameter (black dots indicated by the arrow in Figure 1b, right). No other regions in the entire skin of the upper beak showed comparable Fe^{3+} enrichments.

Electronmicroscopy

At higher magnification the observed opaque granules can be resolved as clusters of extremely fine-grained particles with diameters between 1 and 5 nm. Due to the overall opacity of the clusters in normal bright-field images, it is difficult to distinguish between the particles and a possible surrounding matrix. We there-

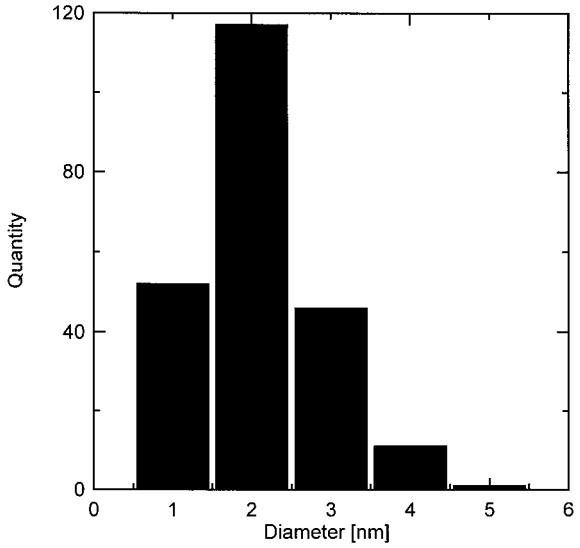

Figure 2. Grain-size distribution of the nanoparticles within the clusters.

Table 1. The d-spacings of magnetite in the pigeon's upper-beak skin (left column) and in *Geobacter metallireducens* (middle column) and the corresponding ASTM-data for magnetite (right columns)

Pigeon (nm)	Geobacter (nm)	ASTM	
		Nm	Intensity
–	0.483	0.485	8
0.29	0.296	0.297	30
0.25	0.252	0.253	100
0.21	0.209	0.2099	20
–	0.170	0.171	10
0.16	0.161	0.162	30
0.15	0.148	0.148	40

fore applied the dark-field imaging technique and thus were able to identify individual nanocrystals. The grain-size histogram (Figure 2) shows a maximum for a particle diameter of 2 nm. The SAED pattern of the particle clusters show a powder diffraction diagram characteristic of fine-grained crystalline material (Figure 3, Table 1). The d-spacings and their corresponding intensities together with the black color of the clusters in the light microscope are diagnostic for magnetite. We did not detect any other magnetite particles outside the clusters, although the entire tissue was scanned thoroughly.

Our detection of magnetite in the pigeon tissue confirms the earlier findings of Walcott *et al.* (1979) and Presti & Petigrew (1980) as described above.

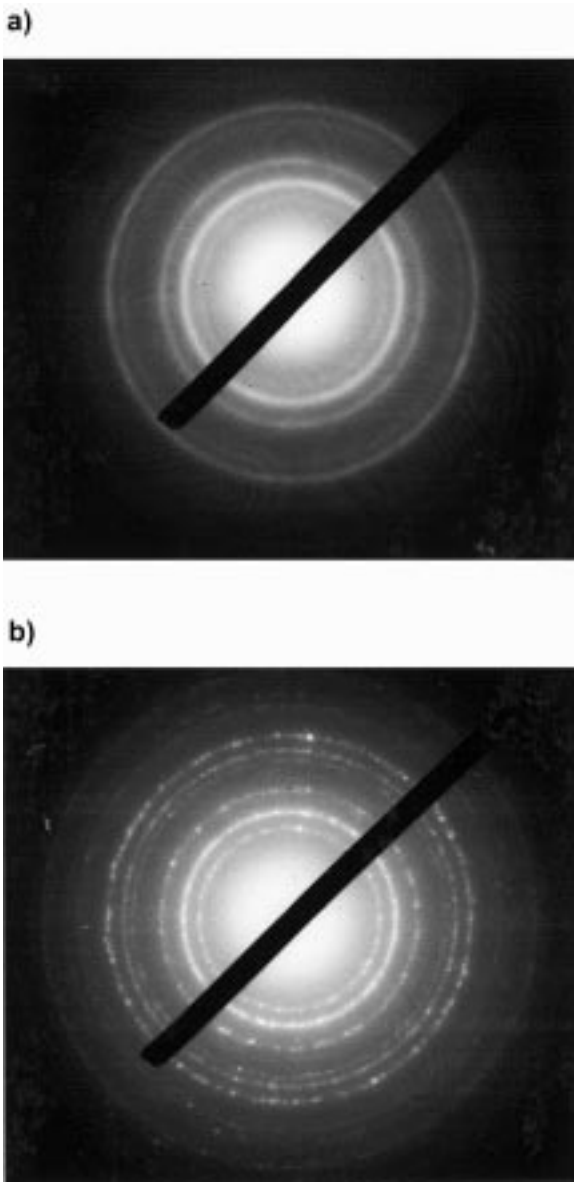

Figure 3. (a) SAED pattern of a particle cluster. Obviously, there are no preferential orientations of the crystal axes in the cluster. (b) SAED pattern of magnetites produced by extracellular bacteria, for comparison. The d-spacings and corresponding intensities are shown in Table 1. This confirms that the Prussian-Blue marked granules consist of clusters of magnetite nanocrystals.

However, the grain size observed here is such that superparamagnetic behavior can be expected for the material at room temperature (Butler & Banerjee 1975, Winklhofer *et al.* 1997). It is important to note that magnetite with grain sizes above 5 nm was not detected in any of the clusters investigated nor elsewhere in the upper-beak skin.

Magnetic properties at room temperature

We obtained a first indication of the presence of ferromagnetic material in the pigeon upper-beak tissue by a series of magnetization measurements with a SQUID magnetometer, conducted in a similar way as described by Walcott *et al.* (1979), or by Presti & Pettigrew (1980). The magnetization was measured in zero field and 1 Oe (maximum field that could be applied in the magnetometer). The fresh unfixed tissue did not show a detectable remanent magnetization, but an induced magnetization when measured in 1 Oe. After approx. 30 min, the tissue changed to a state where it did acquire a remanent magnetic moment (of the order of 10^{-6} emu) when exposed to stepwise increased magnetic fields. These results indicated to us that the fresh tissue must have been changing rapidly its original structure, probably due to desiccation, thereby altering a hypothetical magnetic-particle configuration. As a first interpretation of this phenomenon – though not compelling at this point – we tentatively assumed superparamagnetic particles to agglomerate during the first 30 min, thereby increasing the effective particle size above the threshold size for the transition from SP to stable magnetic behavior. Regarding the distribution of magnetic material, we found that the tissue at all the three parts (proximal, medial, and distal, Figure 1b) displayed a saturation remanent magnetic moment of comparable intensity (between 15 and 30 $\times$ 10^{-6} emu after exposure to a saturation magnetic field of 2000 Oe), which agrees well with our light-microscopic findings.

Low temperature magnetic measurements

Up to 20 K the ZFC-FC-curves (Figure 4a) are in good accordance with superparamagnetic material with blocking temperatures below $T = 5$ K. At higher temperatures (around 140 K) a broad peak is visible, which indicates the presence of an additional magnetic phase. When plotting the magnetic moment versus reciprocal temperature $1/T$, this feature becomes more pronounced (Figure 4b). At applied fields of 100 and 150 Oe, the peak is shifted to slightly higher temperatures ($\sim$160 K). The peak disappears at higher fields between 150 and 200 Oe. An influence of the applied magnetic field on the peak temperature (usually designated blocking temperature, T_B) of ZFC-curves has previously been observed for magnetite (Luo *et al.* 1991) and maghemite (Sappey *et al.* 1997). Luo *et al.* attribute the increase of T_B with H to a dipole-dipole

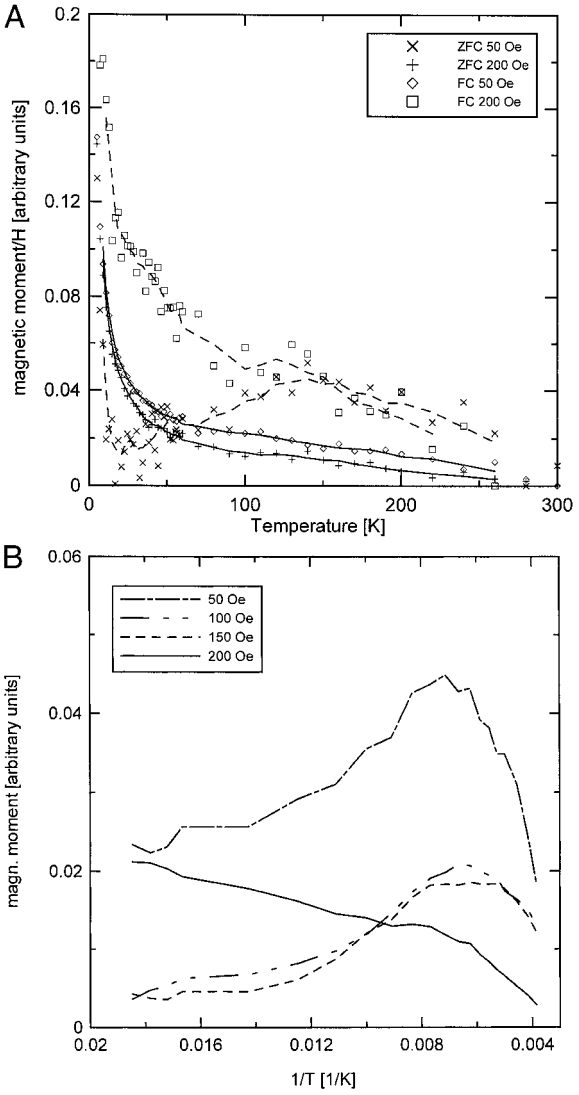

Figure 4. (a) ZFC-FC curves measured in magnetic fields of 50 and 200 Oe. The lines indicate running averages (window width: 5 data points). The data were corrected for the diamagnetic signal of the resin. (b) ZFC curves for different applied fields.

interaction between the particles of a system with random anisotropy. They also observed an increase of the peak temperature with increasing concentration of magnetite particles.

To obtain the distribution of blocking temperatures the remanence curve was differentiated (Figure 5). The data were fitted assuming a log-normal distribution of blocking temperatures as described by Blanco-Mantecón & O'Grady (1999). We have fitted the data with 3 log-normal distributions. The occurrence of a low and an intermediate blocking temperature (3.42

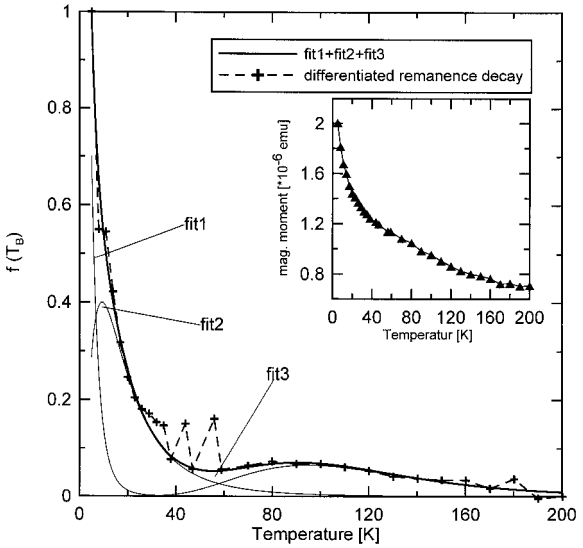

Figure 5. Derivative of the remanence decay and the fitted distribution of blocking temperatures (see also Table 2 for the fitting parameters). Inset: Temperature decay of the remanence.

Table 2. Values for the lognormal distributions of blocking temperatures used to fit the differentiated remanence decay

	$\frac{T_B}{(K)}$	σ	Percentage (%)
Fit 1	3.42	0.75	60.1
Fit 2	17.3	0.78	34.3
Fit 3	108.9	0.37	5.6

and 17.3 K, see Table 2) is consistent with the studies of Blanco-Mantecón & O'Grady (1999) on various systems of synthetic superparamagnetic magnetite nanoparticles. They described a bimodal distribution of blocking temperatures, with the peak at low T_B representing crystals which had not grown beyond the seed stage.

The highest blocking temperature in Table 2 ($T_B =$ 108.9 K) is best explained by a dipole-dipole interaction of densely packed superparamagnetic particles.

Discussion

Together with the electronmicroscopical observation the results of the magnetic measurements can be interpreted as a combination of two effects: (1) The rapid decay of both the remanent and the induced magnetization at low temperatures is an indication of the presence ofvery small superparamagnetic particles. (2) The peak at higher temperatures can be attributed to agglomerated magnetite particles. This interpretation is also supported by the TEM investigations which showed that the distribution of the magnetite particles is not completely homogeneous within the cluster. There are regions with finely dispersed particles on the one hand, and regions with more agglomerated particles on the other.

It is essential to note that neither electronmicroscopic nor magnetic measurements gave any indication of the presence of stable single-domain magnetite in the entire upper-beak skin of homing pigeons.

Acknowledgements

The authors would like to thank Prof. H. Krenn for giving access to the MPMS at the Institut für Halbleiter- und Festkörperphysik in Linz where test measurements were performed. Most of the low temperature measurements were carried out at the Institute for Rock magnetism, University of Minnesota, which is funded by the University of Minnesota, the National Science Foundation and the Keck Foundation. This work was supported by the Volkswagen Foundation.

References

Beason RC, Semm P. 1987 Magnetic responses of the trigeminal nerve system of the bobolink (*Dolichonyx oryzivorous*). *Neurosci Lett* **80**, 229.

Blakemore RP. 1975 Magnetotactic bacteria. *Science* **190**, 377–379.

Blanco-Mantecón M, O'Grady K. 1999 Grain size and blocking distributions in fine particle iron oxide nanoparticles. *J Magn Magn Mater* **203**, 50–53.

Bubien-Waluszewska A. 1981 The cranial nerves. In: *Form and Function in Birds* New York: Academic Press; 385–438.

Butler RF, Banerjee SK. 1975 Theoretical single-domain grain size range in magnetite and titanomagnetite. *J Geophys Res* **80**, 4049–4058.

Holtkamp-Rötzler E. 1998 *Verhaltensphysiologische, physikalische und neuroanatomische Befunde zur Magnetfeldperzeption bei Brieftauben (Columba livia)*. Inaugural-Dissertation (Fachbereich Biologie, Universität Frankfurt) 177 pp.

Ising G. 1945 Die physikalische Möglichkeit eines tierischen Orientierungssinnes auf der Basis der Erdrotation. *Ark Mat Astron Fys* **32A**, 1–23.

Lowenstamm HA. 1962 Magnetite in denticle capping in recent chitons (Polyplacophora). *Geol Soc Am Bull* **73**, 435–438.

Luo W, Nagel SR, Rosenbaum TF, Rosensweig RE. 1991 Dipole interactions with random anisotropy in a frozen ferrofluid. *Phys Rev Lett* **67**, 2721–2724.

Presti D, Pettigrew JD. 1980 Ferromagnetic coupling to muscle receptors as a basis for geomagnetic field sensitivity in animals. *Nature* **285**, 99–101.

Sappey R, Vincent E, Hadacek N, Chaput F, Boilot JP, Zins D. 1997 Nonmonotonic field dependence of the zero-field cooled magnetization peak in some systems of magnetic nanoparticles. *Phys Rev* **B56**, 14551–14559.

Semm P, Nohr D, Demaine C, Wiltschko W. 1984 Neural basis of the magnetic compass: interactions of visual, magnetic and vestibular inputs in the pigeon's brain. *J Comp Physiol* **A155**, 283–288.

Tanka Y, Berschauer JA. 1969 Application of the Pearl's method for iron staining to sections embedded in epoxy resin. *Stain Technol* **44**, 255–256.

Walcott C, Gould JL, Kirschvink JL. 1979 Pigeons have magnets. *Science* **205**, 1027–1029.

Walker MM, Diebel CE, Haugh CV, Pankhurst PM, Montgomery JC, Green CR. 1997 Structure and function of the vertebrate magnetic sense. *Nature* **390**, 371–376.

Wiltschko R, Wiltschko W. 1995 *Magnetic Orientation in Animals.* Berlin: Springer-Verlag.

Winklhofer M, Fabian K, Heider F. 1997 Magnetic blocking temperatures of magnetite calculated with a three-dimensional micromagnetic model. *J Geophys Res* **B102**, 22, 695–22, 709.